Boundary-Layer Meteorol (2007) 125:525–536
DOI 10.1007/s10546-007-9203-8

ORIGINAL PAPER

Modelling mean and turbulence fields in the dry convective boundary layer with the eddy-diffusivity/mass-flux approach

Peter Hurley

Received: 15 January 2007 / Accepted: 29 May 2007 / Published online: 28 June 2007

Abstract The treatment of turbulence closure in atmospheric models is examined in the context of the dry convective boundary layer (CBL) and the eddy-diffusivity/mass-flux (EDMF) approach. The EDMF approach is implemented into a model called TAPM to use a coupled two-equation prognostic turbulence closure and the mass-flux approach to represent turbulence in the CBL. This work also extends the range of turbulence variables that can be derived from the mass-flux component of the model and uses these along with their values from the prognostic scheme to provide total turbulence fields that can be used to compare to data and/or to feed into other components of TAPM, including those needed to drive Eulerian and Lagrangian air pollution dispersion modules. Model results are presented for the afternoon of a simulated summer day and are compared to both laboratory and field observations in a mixed-layer scaled framework. The results show that the EDMF approach works well within TAPM and can provide good predictions of mean and turbulence fields, including in the upper levels of the CBL. The EDMF approach has several attractive features, including the potential to be one approach to unify the treatment of turbulence and dry and moist convection in atmospheric models.

Keywords Convection · Convective boundary layer · EDMF · TAPM · Turbulence

1 Introduction

The turbulence closure problem and its representation in the Reynolds averaged equations used in atmospheric models has attracted much attention over many decades. One of the most common approaches, particularly in global and mesoscale numerical models, is to use a first-order gradient-diffusion approach to close the equations with (optionally) a non-local or counter-gradient term for scalar fluxes to represent the largest eddies in the convective boundary layer (CBL). The counter-gradient term is usually represented by either a constant (e.g.

P. Hurley (✉)
CSIRO Marine and Atmospheric Research, PMB #1, Aspendale, VIC 3195, Australia
e-mail: Peter.Hurley@csiro.au

Hurley 1997), a value that depends on mixed-layer scaling (e.g. Holtslag and Boville 1993), or by a value that depends on scalar variances that may themselves be based on second-order turbulence closure equations (e.g. Andren 1990).

A recently developed alternative method to represent turbulence in the convective boundary layer is one that parameterises the vertical flux of a scalar as the sum of a gradient-diffusion term to represent the small-scale eddies and a mass-flux term to represent the large-scale convective eddies. Siebesma and Teixeira (2000) and Teixeira and Siebesma (2000) used this approach in the ECMWF global model together with a profile-specified eddy-diffusivity closure, while Soares et al. (2004) used this approach, referred to as the eddy-diffusivity/mass-flux (EDMF) method, together with an existing $E-l$ one-equation prognostic turbulence model within the mesoNH model.

Jakob and Siebesma (2003) used the mass-flux and updraft model approach to simulate moist convective processes, including as a simple but effective framework to trigger moist convection and to calculate parcel ascent and condensation. Soares et al. (2004) treated both dry and moist convection in the EDMF framework, and demonstrated that this approach has the potential to represent turbulence processes in dry and moist convection within a unified approach rather than as separately parameterised processes.

In this study we use the EDMF approach for the dry convective boundary layer, but using a two-equation prognostic turbulence equation model within The Air Pollution Model (TAPM; Hurley 2005a, b), combined with the mass-flux model from Soares et al. (2004). As we also need to predict other turbulence variables that are used to drive the air pollution component of TAPM, we will also develop and use parameterisations for the contribution of the two EDMF components to the velocity variances and the eddy dissipation rate that feed into the Lagrangian particle module used in TAPM to represent point source dispersion. Section 2 of this paper presents a brief overview of TAPM with an emphasis on the existing turbulence model and Sect. 3 presents a description of the modifications made to TAPM to utilise the EDMF approach. Section 4 presents model results for a simulation of the convective boundary layer and compares results to some laboratory and field observations, and Sect. 5 gives conclusions.

2 An overview of TAPM

The modelling framework used for this study is TAPM V3.5, which is an updated version of V3 and V2 described in Hurley (2005a) and Hurley et al. (2005a), respectively, with a complete technical description of the V3 model equations, parameterisations, and numerical methods described in Hurley (2005b), and a summary of some verification studies given in more detail in Hurley et al. (2005b).

TAPM uses the fundamental equations of atmospheric flow, thermodynamics, moisture conservation, turbulence and dispersion, wherever practical, for horizontal modelling domains of up to about 1,500 km in size and horizontal grid spacing typically from 30 km down to 300 m for meteorology. For computational efficiency, it includes a nested approach for meteorology and air pollution, with the pollution grids optionally able to be configured for a sub-region and/or at finer grid spacing than the meteorological grid, which allows a user to rapidly zoom-in to a local region of interest. The meteorological component of the model is nested within synoptic-scale analyses/forecasts that drive the model at the boundaries of the outer grid. The coupled approach taken in the model, whereby mean meteorological and turbulence fields are passed to the air pollution module every 5 min, allows pollution modelling to be done accurately during rapidly changing conditions such as those that occur

in sea-breeze or frontal situations, or in complex terrain. The use of integrated plume rise, Lagrangian particle, building wake, and Eulerian grid modules, allows industrial plumes to be modelled accurately at fine resolution for long simulations. Similarly, the use of a condensed chemistry scheme also allows nitrogen dioxide, ozone, and particulate mass to be modelled for long periods for industrial or urban regions.

TAPM has been verified for a number of Australian and international datasets, including for coastal meteorology and shoreline fumigation in Kwinana near Perth, Australia (Hurley et al. 2001); urban and coastal meteorology and photochemical air pollution in Melbourne, Australia (Hurley et al. 2003a); rural and urban meteorology and tall-stack dispersion for the Kincaid and Indianapolis international model inter-comparison datasets (Luhar and Hurley 2003); coastal meteorology and photochemical dispersion from an LNG Plant in the Pilbara region of northern Australia (Hurley et al. 2003b); meteorology and tall-stack dispersion in complex terrain in Anglesea, Victoria, Australia (Hill and Hurley 2003), Lovett and Westvaco in the U.S.A. (Hurley 2005a); for dispersion within building downwash for Bowline U.S.A. (Hurley 2005a); and for two evaluation studies of predicted vertical profiles of winds against SODAR observations for Kalgoorlie in Western Australia (Edwards et al. 2004) and for the Pilbara (Physick et al. 2004). Results from these studies have shown good model performance for both meteorology and air pollution predictions, particularly for the study of annual extreme (high) concentrations important for environmental impact assessments.

The enhanced version of TAPM (V3.5) used here has been modified to include a number of options, including the use of more complete land-surface schemes and global datasets for soil and vegetative canopies. Results from this version have been re-run on a number of the above field datasets, with overall similarly good results (compared to V3) for meteorology and air pollution, but with some noticeable improvements to surface fluxes and near-surface meteorology.

In this paper TAPM is used in a single column model (SCM) mode, with a focus on the mean and turbulent structure of the afternoon dry convective boundary layer. As such, the three-dimensional (3D) complexity of the model is irrelevant for this study and the mean equations condense to simple 1D equations for momentum, potential virtual temperature, specific humidity and turbulence equations. The pressure is hydrostatic and the vertical velocity is zero. All of the model equations and parameterisations are not presented here (they can be seen in detail in the TAPM references above), however a summary of the turbulence closure is presented (in its simple 1D form relevant here)—note that an earlier version of this closure was compared to nine other turbulence closures for the convective boundary layer and for some other flows by Hurley (1997), and was referred to as Model 10 in that paper.

Turbulence closure in the mean equations uses a gradient diffusion approach, which depends on a diffusion coefficient K and gradients of mean variables. The vertical fluxes for momentum and potential virtual temperature are

$$\overline{u'w'} = -K\frac{\partial u}{\partial z}, \tag{1}$$

$$\overline{v'w'} = -K\frac{\partial v}{\partial z}, \tag{2}$$

$$\overline{w'\theta_v'} = -K\left(\frac{\partial \theta_v}{\partial z} - \gamma_{\theta_v}\right), \tag{3}$$

where γ_{θ_v} represents a counter-gradient term and is set to a constant value of $\gamma_{\theta_v} = 0.00065$ $\mathrm{K\,m^{-1}}$, from Deardorff (1966).

The turbulence scheme used to calculate K is the standard E–ε model, with production terms and some constants for the eddy dissipation rate equation derived from the analysis of Duynkerke (1988). The model solves prognostic equations for the turbulence kinetic energy (E) and the eddy dissipation rate (ε)

$$\frac{\mathrm{d}E}{\mathrm{d}t} = \frac{\partial}{\partial z}\left(K\frac{\partial E}{\partial z}\right) + P_s + P_b - \varepsilon, \tag{4}$$

$$\frac{\mathrm{d}\varepsilon}{\mathrm{d}t} = \frac{\partial}{\partial z}\left(c_{\varepsilon 0}K\frac{\partial \varepsilon}{\partial \sigma}\right) + \frac{\varepsilon}{E}\left(c_{\varepsilon 1}\left(P_s + \max(0, P_b) + \max(0, P_T)\right) - c_{\varepsilon 2}\varepsilon\right), \tag{5}$$

where

$$P_s = K\left(\left(\frac{\partial u}{\partial z}\right)^2 + \left(\frac{\partial v}{\partial z}\right)^2\right),$$

$$P_b = -\frac{g}{\theta_v}K\left(\frac{\partial \theta_v}{\partial z} - \gamma_{\theta_v}\right),$$

$$P_T = \frac{\partial}{\partial z}\left(K\frac{\partial E}{\partial z}\right),$$

and $K = c_m\dfrac{E^2}{\varepsilon}$, $c_m = 0.09$, $c_{\varepsilon 0} = 0.69$, $c_{\varepsilon 1} = 1.46$ and $c_{\varepsilon 2} = 1.83$.

TAPM also has an option for an E–l approach that uses a diagnostic length scale, and thus a diagnostic eddy dissipation rate, but this option is not used here.

Turbulence boundary conditions are specified at the first model level using surface and mixed layer scaling. The convective velocity scale w_* has its usual definition and the CBL height (z_i) is defined as the first model level above the surface for which the vertical heat flux is negative.

Turbulence kinetic energy and eddy dissipation rate are enhanced in the top half of the CBL, where turbulence levels can be underestimated using the above approaches. This has been achieved in TAPM by using a simple parameterisation that limits the rate of decrease of prognostic turbulence with height, between heights in the range 0.55–0.95 times the CBL height.

Vertical velocity variance $\overline{w'^2}$ is diagnosed from the prognostic equation of Gibson and Launder (1978) and Andren (1990) by neglecting advection and diffusion terms

$$\overline{w'^2} = \left(\frac{2}{3}E + \frac{E}{c_{s1}\varepsilon}\left((2 - c_{s2} - c_{w2}\frac{l}{kz})P_s + (2 - c_{s3} - c_{w3}\frac{l}{kz})P_b - \frac{2}{3}\varepsilon\right)\right). \left(1 + \frac{c_{w1}}{c_{s1}}\frac{l}{kz}\right)^{-1}, \tag{6}$$

with constants from Rodi (1985)

$$c_{s1} = 2.20, \quad c_{s2} = 1.63, \quad c_{s3} = 0.73, \quad c_{w1} = 1.00, \quad c_{w2} = 0.24, \quad c_{w3} = 0.0.$$

The horizontal velocity variance is diagnosed from E and $\overline{w'^2}$. The velocity variances and eddy dissipation rate feed directly into the air pollution component of the model to drive the Lagrangian Particle Module (LPM) that represents dispersion from point sources, while the eddy diffusivity is used by the Eulerian Grid Module (EGM).

3 Extension of TAPM to use the EDMF approach

The extended model evaluated herein is the same as that described in Sect. 2, but using the EDMF approach with the counter-gradient term in the vertical heat flux equation parameterised using a mass-flux scheme following Soares et al. (2004)

$$\overline{w'\theta'_v} = -K\left(\frac{\partial\theta_v}{\partial z} - \gamma_{\theta_v}\right) \equiv -K\frac{\partial\theta_v}{\partial z} + M\left(\theta_{v,up} - \theta_v\right), \tag{7}$$

resulting in $\gamma_{\theta_v} = M(\theta_{v,up} - \theta_v)/K$, and where $M = a_{up}w_{up}$ is the mass flux ($\mathrm{m\,s^{-1}}$), $\theta_{v,up}$ is the virtual potential temperature (K) in the convective updraft, obtained from

$$\frac{\partial\theta_{v,up}}{\partial z} = \varepsilon_E\left(\theta_{v,up} - \theta_v\right), \tag{8}$$

w_{up} is the vertical velocity ($\mathrm{m\,s^{-1}}$) in the convective updraft, obtained from

$$\frac{1}{2}\frac{\partial w_{up}^2}{\partial z} = -\varepsilon_E b_1 w_{up}^2 + b_2\frac{g}{\theta_v}\left(\theta_{v,up} - \theta_v\right), \tag{9}$$

with $a_{up} = 0.1$, $b_1 = 1$, $b_2 = 2$, $\varepsilon_E = 0.5\left(\frac{1}{z+\Delta z} + \frac{1}{\max(0,z_i-z)+\Delta z}\right)$, and boundary conditions $\theta_{v,up} = \theta_v + \frac{\overline{w'\theta'_v}\big|_0}{E^{1/2}}$ at the first model level and $w_{up} = 0$ at the surface.

These equations are integrated with increasing height using an implicit discretisation, and the CBL height (z_i) is diagnosed as the first model level where the updraft velocity decreases to zero. In order to aid numerical stability, particularly in the early-morning shallow CBL, the value of γ_{θ_v} is kept within the range of zero and $0.002\,\mathrm{K\,m^{-1}}$ (approximately three times the constant value used in the base model described in Sect. 2).

The mass-flux approach also allows the calculation of the contribution of the large convective eddies to the vertical velocity variance and the Lagrangian time scale, following the analyses of deRoode et al. (2000)

$$\left(\overline{w'^2}\right)_{MF} = 4M^2, \tag{10}$$

$$(T_L)_{MF} = \frac{1}{5M\varepsilon_E}, \tag{11}$$

where the subscript MF refers to the mass-flux contribution (note that in Eq. 11 we have assumed that detrainment is 1.5 times entrainment, consistent with the mass-flux approach). The eddy dissipation rate can then be calculated as

$$(\varepsilon)_{MF} = \frac{\left(\overline{w'^2}\right)_{MF}}{(T_L)_{MF}} = 20M^3\varepsilon_E, \tag{12}$$

and consistent with the formulation of the eddy diffusivity from the previous section, the corresponding eddy diffusivity can be calculated using

$$(K)_{MF} = c_m\frac{\left(\frac{1}{2}\overline{w'^2}\right)^2_{MF}}{(\varepsilon)_{MF}} = \frac{c_m M}{5\varepsilon_E}. \tag{13}$$

The total vertical velocity variance, eddy dissipation rate and eddy diffusivity is then just the sum of the contributions from the gradient closure (Sect. 2) and the mass-flux contribution.

Note that the use of the total diffusivity for a scalar would only be required if the turbulence closure for the scalar flux (e.g. pollution concentration in EGM mode in TAPM) does not explicitly include a counter-gradient flux term.

4 Model results for the dry convective boundary layer

TAPM was configured in SCM mode with non-time varying 1D synoptic profiles of wind speed ($5\,m\,s^{-1}$), westerly wind direction, a surface potential temperature of 290 K with a vertical gradient of $0.005\,K\,m^{-1}$ up to 2,000 m and $0.010\,K\,m^{-1}$ above, and a specific humidity of 0.007 $kg\,kg^{-1}$ at the surface decreasing to zero at 5,000 m. The vertical model resolution used is the default 25 levels with heights of 10, 25, 50, 100, 150, 200, 250, 300, 400, 500, 600, 750, 1,000, 1,250, 1,500, 1,750, 2,000, 2,500, 3,000, 3,500, 4,000, 5,000, 6,000, 7,000 and 8,000 m. The model was run for a mid-latitude summer day with a 5 min timestep, for a diurnal cycle starting at midnight and with land-surface type set to grassland with sandy-clay-loam soil. The model output is presented at 1400 LST. Note that at this time the boundary-layer height was 1,500 m and was increasing at a rate of about $250\,m\,h^{-1}$, the friction velocity scale was $0.45\,m\,s^{-1}$, the virtual potential temperature scale was -0.86 K, and the convective velocity scale was $2.56\,m\,s^{-1}$.

Figures 1–3 show model simulations at 1400 LST for a number of variables and also shown are the laboratory data of Deardorff and Willis (1985) (D&W) and Hibberd and Sawford (1994) (H&S) (see also Luhar et al. 1996), as well as the atmospheric data of Caughy and Palmer (1979) (C&P) and Young (1988). All turbulence quantities are presented in non-dimensional form using surface-layer or mixed-layer scaling, as is the height. Note that the H&S horizontal velocity variance shown in Fig. 2 has been updated since publication of the H&S paper, with a revised analysis method used to correct a bias in the original analysis near the surface (M. Hibberd 2006, personal communication). Note that the atmospheric data generally show a large degree of scatter, whereas the H&S data and to a lesser extent the D&W data show much less scatter, as they represent an ensemble average and so can be compared more directly against model results that implicitly represent an ensemble average due to Reynolds averaging of the model equations.

Figure 1 shows the virtual potential temperature and (scaled) virtual potential temperature vertical flux versus (scaled) height. The results indicate that the virtual potential temperature profile is as expected for the CBL, with a negative gradient in the bottom half of the CBL that decreases with height to then be a positive gradient in the top half of the profile, and then leading to a stronger positive gradient above the CBL. The vertical flux profile shows the expected linear gradient with height with a negative flux at the CBL height. The H&S laboratory tank data shown on the plot indicate similar behaviour, but with a smaller magnitude of the negative flux at the CBL top, whereas C&P field data are a little less overall than both the model and the laboratory data. The modelled minimum (scaled) value of -0.20 is very close to the large-eddy simulation generated profile shown in Soares et al. (2004). The contribution of the mass-flux component to the vertical flux profile is also shown on the plot for reference, and as expected it shows that the counter-gradient term makes a significant contribution to the total flux in the middle and upper part of the CBL in the current formulation.

Figure 2 shows the (scaled) horizontal and vertical velocity variances versus (scaled) height. The results show that the horizontal velocity variance is predicted well compared to the H&S data, although the magnitude of the maximum horizontal velocity variance seems to be somewhat underpredicted just below the mixing height. However, this underprediction is actually due to an artefact in the laboratory data that is caused by the very strong stability

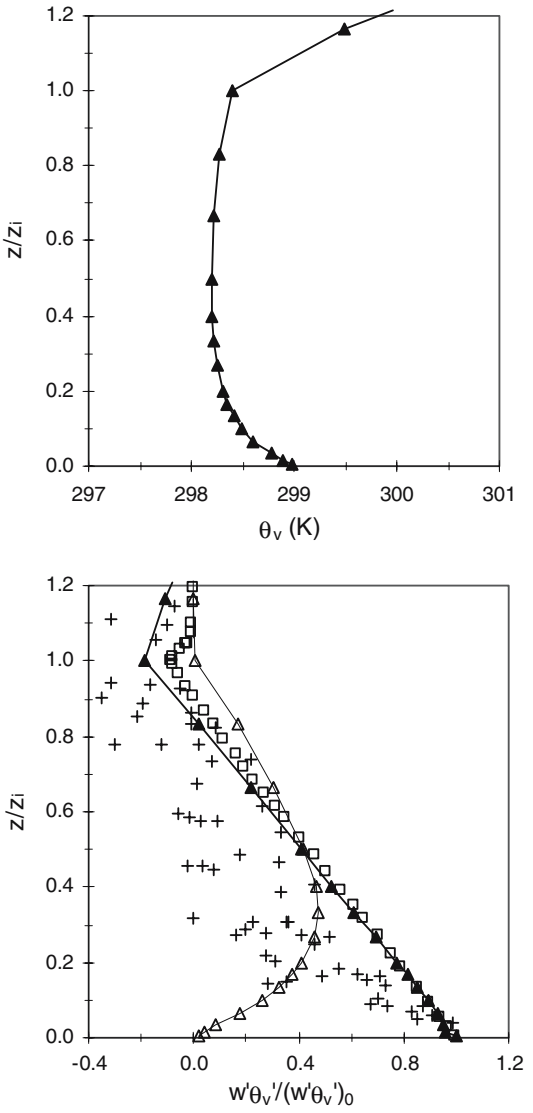

Fig. 1 Predicted (model) virtual potential temperature (top) and scaled virtual potential temperature vertical flux (bottom) versus scaled height. Also shown are various laboratory and field measurements and the predicted contribution of the mass-flux approach, where available. The model simulation at 1400 LST is shown as a *solid line* with filled triangles; the mass-flux component is shown as a *dashed line* with *open triangles*; the laboratory data of Deardorff and Willis (1985) (D&W) are shown as *open circles*; the laboratory data of Hibberd and Sawford (1994) (H&S) (see also Luhar et al. 1996) are shown as *open squares*; and the atmospheric data of Caughey and Palmer (1979) (C&P) and Young (1988) are shown as *pluses* and *crosses*, respectively

effectively used in the laboratory experiments (D&W and H&S) that tends to make a stronger than normal 'lid' on the CBL, and which tends to force the large-scale convective eddies to flow horizontally faster over a smaller depth than normally found in the real atmospheric CBL (M. Hibberd 2006, personal communication). This is confirmed somewhat, although there is a lot of scatter, by the field measurements of C&P, as the H&S data are at the top end

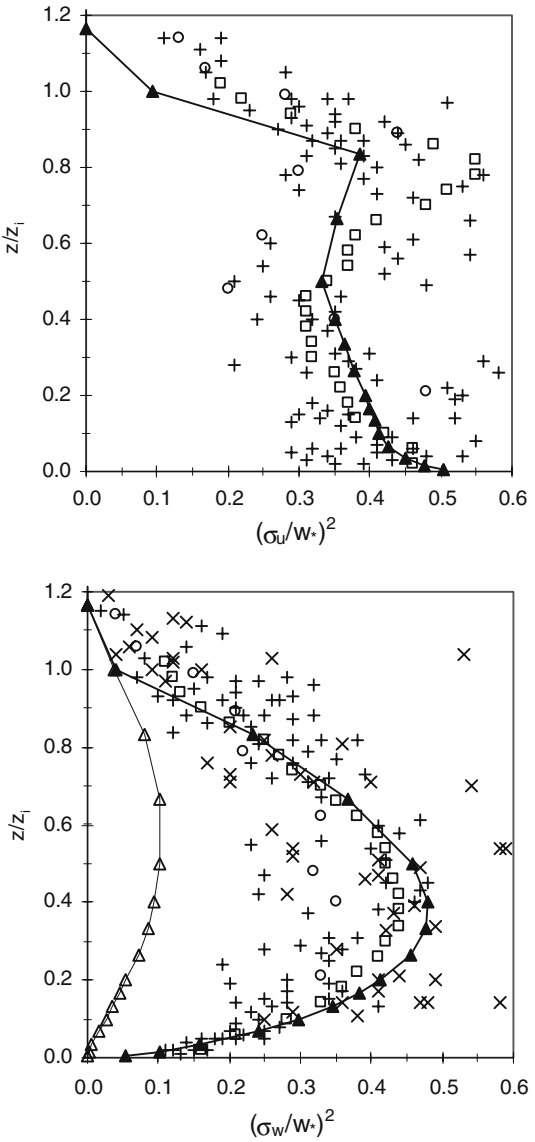

Fig. 2 Predicted (model) scaled horizontal (top) and vertical (bottom) velocity variances versus scaled height. Also shown are various laboratory and field measurements and the predicted contribution of the mass-flux approach, where available. The model simulation at 1400 LST is shown as a *solid line* with *filled triangles*; the mass-flux component is shown as a *dashed line* with *open triangles*; the laboratory data of Deardorff and Willis (1985) (D&W) are shown as *open circles*; the laboratory data of Hibberd and Sawford (1994) (H&S) (see also Luhar et al. 1996) are shown as *open squares*; and the atmospheric data of Caughey and Palmer (1979) (C&P) and Young (1988) are shown as *pluses* and *crosses*, respectively

of the field data range. The modelled vertical velocity variance is also modelled well as it is very close to the H&S data and is near the middle of the range of the field data. It can also be seen that the mass-flux component of the vertical velocity variance makes an important contribution to the total variance, especially in the upper part of the CBL. Both the horizontal and vertical velocity variances seem a little smaller than those for data at the mixing height,

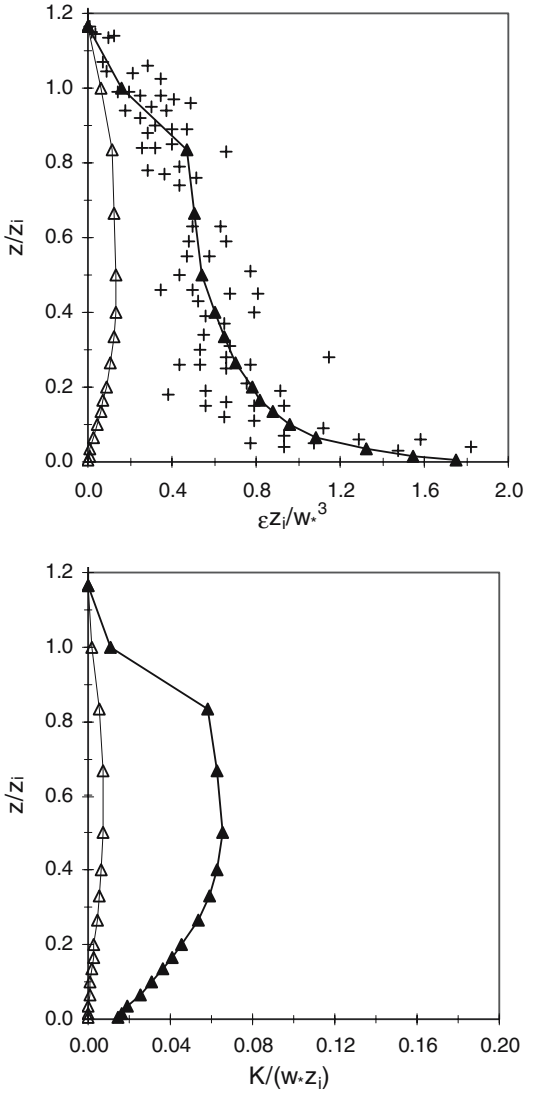

Fig. 3 Predicted (model) scaled eddy dissipation rate (top) and eddy diffusivity (bottom) versus scaled height. Also shown are various laboratory and field measurements and the predicted contribution of the mass-flux approach, where available. The model simulation at 1400 LST is shown as a *solid line* with *filled triangles*; the mass-flux component is shown as a *dashed line* with *open triangles*; the laboratory data of Deardorff and Willis (1985) (D&W) are shown as *open circles*; the laboratory data of Hibberd and Sawford (1994) (H&S) (see also Luhar et al. 1996) are shown as *open squares*; and the atmospheric data of Caughey and Palmer (1979) (C&P) and Young (1988) are shown as *pluses* and *crosses* respectively

but this may be partly due to the coarser grid spacing used at these heights (250 m), and it may also be partly due to the mass-flux model only accounting for vertical motion and ignoring horizontal motion that is known to be important near the mixing height.

Figure 3 shows the predicted (scaled) eddy dissipation rate and eddy diffusivity versus (scaled) height. The results show that the eddy dissipation rate compares well with the field data of C&P. The eddy diffusivity profile shows that a similar amount of diffusion is effectively

occurring throughout the bulk of the modelled CBL, as would be expected when considering the range of eddy sizes occurring in the CBL. The contribution of the mass-flux term to the eddy dissipation rate is quite small, while it is a little larger for the eddy diffusivity.

In comparing the above results with those shown by Hurley (1997) using the old scheme, it can be seen that while the turbulence fields are similar in the lower part of the CBL, the fields in the upper part of the CBL are slightly better with the new scheme. The fact that the old scheme turbulence profiles look reasonably good is partly due to a non-conventional definition of using a CBL height that is defined as the height where the vertical heat flux is zero, rather than the usual definition of the CBL height as the height where the vertical heat flux is at its minimum. If we had used the more conventional (proper) definition of the CBL height in the old scheme, then the turbulence in the upper part of the CBL would have been severely underestimated when viewed in a convectively scaled framework. As a consequence of the definition of the mixing height used by the old scheme, the heat flux profile had its minimum value in a convectively scaled framework above the CBL height, and the potential temperature profile also suffered from problems just above the CBL height. The new scheme alleviates the above problems suffered by the old scheme by providing a calculation of the CBL height that is consistent with the proper minimum heat flux profile definition of this height, while providing a physical framework that enables the simulation of those parts of the turbulence profiles due to the large eddies of the CBL provided by the mass-flux scheme to enhance turbulence in the middle and upper parts of the CBL. The result of using this approach leads to a consistent and good description of mean and turbulence variables in the CBL.

5 Conclusions

The work presented here explores the usefulness of the EDMF approach for the dry convective boundary layer in the context of a mass-flux approach to represent the large-scale convective eddies and a two-equation prognostic approach to represent the smaller scale turbulence. This work builds on the EDMF concept to also calculate other turbulence quantities such as velocity variances, eddy dissipation rate and effective eddy diffusivity that could be used to drive both Eulerian and Lagrangian air pollution modules. The model results presented in a mixed-layer scaled framework for the convective boundary layer compare well with both laboratory and field data, and complement the previous comparison to large-eddy simulations performed by Soares et al. (2004).

The attractiveness of this approach is that it is conceptually simple and easy to code into existing counter-gradient terms in atmospheric models for various levels of turbulence closure ranging from first-order diagnostic K models to one- and two-equation turbulence kinetic energy models, without the need to introduce even higher-order closure approaches. The other very attractive feature, as demonstrated by Soares (2004), is that the EDMF approach is ideally suited to unify the interaction of turbulence and dry and moist convection that is currently treated by separate approaches in most atmospheric models, and this will be an area of future research.

Acknowledgements Thanks to Mark Hibberd for providing the laboratory and field data and for his advice on the use of these data and to Ashok Luhar and two external reviewers for helpful comments on the manuscript.

This work was funded by CSIRO Marine and Atmospheric Research and the Australian Greenhouse Office as a science contribution to the new Australian Community Climate and Earth System Simulator (ACCESS) initiative (a joint initiative with the Australian Bureau of Meteorology Research Centre).

References

Andren A (1990) Evaluation of a turbulence closure scheme suitable for air pollution applications. J Appl Meteorol 29:224–239

Caughey S, Palmer S (1979) Some aspects of turbulence structure through the depth of the convective boundary layer. Quart J Roy Meteorol Soc 105:811–827

Deardorff J (1966) The counter-gradient heat flux in the lower atmosphere and in the laboratory. J Atmos Sci 23:503–506

Deardorff J, Willis G (1985) Further results from a laboratory model of the convective boundary layer. Boundary-Layer Meteorol 32:205–236

deRoode S, Duynkerke P, Siebesma A (2000) Analogies between mass-flux and Reynolds-averaged equations. J Atmos Sci 57:1585–1598

Duynkerke P (1988) Application of the E–ε turbulence closure model to the neutral and stable atmospheric boundary layer. J Atmos Sci 45:865–880

Edwards M, Hurley P, Physick W (2004) Verification of TAPM meteorological predictions using sodar data in the Kalgoorlie region. Aust Met Mag 53:29–37

Gibson M, Launder B (1978) Ground effects on pressure fluctuations in the atmospheric boundary layer. J Fluid Mech 86:491–511

Hibberd M, Sawford B (1994) A saline laboratory model of the planetary convective boundary layer. Boundary-Layer Meteorol 67:229–250

Hill J, Hurley P (2003) The use of TAPM at Anglesea. Proceedings of the national clean air conference of CASANZ. Newcastle, Australia 23–27 November 2003

Holtslag A, Boville B (1993) Local versus non-local boundary-layer diffusion in a global climate model. J Climate 6:1825–1842

Hurley P (1997) An evaluation of several turbulence schemes for the prediction of mean and turbulent fields in complex terrain. Boundary-Layer Meteorol 83:43–73

Hurley P (2005a) TAPM V3—model description and verification. Clean Air 39:32–36

Hurley P (2005b) The air pollution model (TAPM) version 3. Part 1: Technical description. CSIRO Atmospheric Research Technical Paper No. 71

Hurley P, Blockley A, Rayner K (2001) of a prognostic meteorological and air pollution model for year-long predictions in the Kwinana region of Western Australia. Atmos Environ 35:1871–1880

Hurley P, Manins P, Lee S, Boyle R, Ng Y, Dewundege P (2003a) Year-long, high-resolution, urban airshed modelling: Verification of TAPM predictions of smog and particles in Melbourne, Australia. Atmos Environ 37:1899–1910

Hurley P, Physick W, Cope M, Borgas M, Brace P (2003b) An evaluation of TAPM for photochemical smog applications in the Pilbara region of WA. Proceedings of the national clean air conference of CASANZ, Newcastle, Australia, 23–27 November 2003

Hurley P, Physick W, Luhar A (2005a) TAPM—A practical approach to prognostic meteorological and air pollution modelling. Environ Modell & Software 20:737–752

Hurley P, Physick W, Luhar A, Edwards M (2005b) The air pollution model (TAPM) version 3. Part 2: Summary of some verification studies. CSIRO Atmospheric Research Technical Paper No. 72

Jakob C, Siebesma A (2003) A new subcloud model for mass-flux convection schemes: Influence on triggering, updraft properties and model climate. Mon Wea Rev 131:2765–2778

Luhar A, Hurley P (2003) Evaluation of TAPM, a prognostic meteorological and air pollution model, using urban and rural point-source data. Atmos Environ 37:2795–2810

Luhar A, Hibberd M, Hurley P (1996) Comparison of closure schemes used to specify the velocity pdf in Lagrangian stochastic dispersion models for convective conditions. Atmos Environ 30:1407–1418

Physick WL, Rayner KN, Mountford P, Edwards M. (2004) Observations and modelling of dispersion meteorology in the Pilbara region. Aust Met Mag 53:175–187

Rodi W (1985) Calculation of stably stratified shear-layer flows with a buoyancy-extended k–ε turbulence model. In: Hunt JCR (ed) Turbulence and diffusion in stable environments. Clarendon Press, Oxford, pp 111–143

Soares P, Miranda P, Siebesma A, Teixeira J (2004) An eddy-diffusivity/mass-flux parameterisation for dry and shallow cumulus convection. Quart J Ray Meteorol Soc 130:3365–3383

Siebesma A, Teixeira J (2000) An advection-diffusion scheme for the convective boundary layer: description and 1D results. 14th symposium on boundary layer turbulence, 7–11 August 2000, Aspen, Colorado, USA, pp 133–136. American Meteorological Society

Teixeira J, Siebesma A (2000) A mass-flux/K-diffusion approach to the parameterisation of the convective boundary layer: Global model results. 14th Symposium on Boundary Layer Turbulence, 7–11 August 2000, Aspen, Colorado, USA, pp 231–234. American Meteorological Society

Young G (1988) Turbulence structure of the convective boundary layer. Part I: Variability of normalised turbulence statistics. J Atmos Sci 45:719–726